ACS Chemical Neuroscience

Research Article

pubs.acs.org/chemneuro

Synthesis and Evaluation of Translocator 18 kDa Protein (TSPO) Positron Emission Tomography (PET) Radioligands with Low Binding Sensitivity to Human Single Nucleotide Polymorphism rs6971

Paolo Zanotti-Fregonara,[†] Yi Zhang,[†] Kimberly J. Jenko,[†] Robert L. Gladding,[†] Sami S. Zoghbi,[†] Masahiro Fujita,[†] Gianluca Sbardella,[‡] Sabrina Castellano,[‡] Sabrina Taliani,[§] Claudia Martini,[§] Robert B. Innis,[†] Federico Da Settimo,[§] and Victor W. Pike*[,†]

[†]Molecular Imaging Branch, National Institute of Mental Health, National Institutes of Health, Bethesda, Maryland 20892-0001, United States

[‡]Department of Pharmacy, University of Salerno, 84084 Fisciano (SA), Italy

[§]Department of Pharmacy, University of Pisa, Via Bonanno 6, 56126 Pisa, Italy

Supporting Information

ABSTRACT: The imaging of translocator 18 kDa protein (TSPO) in living human brain with radioligands by positron emission tomography (PET) has become an important means for the study of neuroinflammatory conditions occurring in several neuropsychiatric disorders. The widely used prototypical PET radioligand [^{11}C](*R*)-PK 11195 ([^{11}C](*R*)-**1**; [*N-methyl*-^{11}C](*R*)-*N-sec*-butyl-1-(2-chlorophenyl)-*N*-methylisoquinoline-3-carboxamide) gives a low PET signal and is difficult to quantify, whereas later generation radioligands have binding sensitivity to a human single nucleotide polymorphism (SNP) rs6971, which imposes limitations on their utility for comparative quantitative PET studies of normal and diseased subjects. Recently, azaisosteres of **1** have been developed with improved drug-like properties, including enhanced TSPO affinity accompanied by moderated lipophilicity. Here we selected three of these new ligands (**7**–**9**) for labeling with carbon-11 and for evaluation in monkey as candidate PET radioligands for imaging brain TSPO. Each radioligand was readily prepared by ^{11}C-methylation of an *N*-desmethyl precursor and was found to give a high proportion of TSPO-specific binding in monkey brain. One of these radioligands, [^{11}C]**7**, the direct 4-azaisostere of **1**, presents many radioligand properties that are superior to those reported for [^{11}C]**1**, including higher affinity, lower lipophilicity, and stable quantifiable PET signal. Importantly, **7** was also found to show very low sensitivity to the human SNP rs6971 in vitro. Therefore, [^{11}C]**7** now warrants evaluation in human subjects with PET to assess its utility for imaging TSPO in human brain, irrespective of subject genotype.

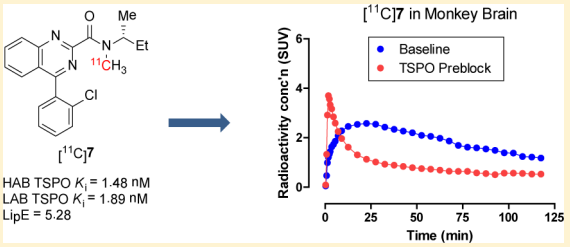

KEYWORDS: *TSPO, PET, radioligand, carbon-11, imaging, brain*

Translocator protein 18 kDa (TSPO), formerly known as the peripheral benzodiazepine receptor,[1] is mainly located in outer mitochondrial membranes[2] and is implicated in several functions, including cholesterol transport and stereoidogenesis.[3−5] TSPO expression is up-regulated in several human pathologies with inflammation, including a large number of neuropsychiatric disorders that are known or suspected to have inflammation.[6−12] In neuroinflammatory conditions, TSPO is upregulated both in activated microglia, which reflect an acute response to injury, and in reactive astrocytes, which may accumulate to form a sclerosis (i.e., scar) in brain and remain for life.[13,14] Thus, PET imaging of TSPO is keenly pursued for its ability to inform on the development of neuroinflammatory conditions in brain and as a potential biomarker in clinical trials with anti-inflammatory drugs.[15−18]

The prototypical radioligand, [^{11}C]PK11195 ([^{11}C]**1**), first as racemate[19,20] and later as its higher affinity *R*-enantiomer ([^{11}C](*R*)-**1**, Figure 1),[21,22] has been used for almost three decades for imaging brain TSPO with PET. However, this radioligand is recognized to have severe limitations, including low sensitivity and poor amenability to quantification.[23] Consequently, considerable efforts have been expended on developing improved radioligands,[15−17] such as [^{11}C]PBR28 ([^{11}C]**2**),[24−26] [^{18}F]FBR ([^{18}F]**3**),[27] [^{11}C]DPA 713 ([^{11}C]**4**),[28] [^{18}F]PBR111 ([^{18}F]**5**),[29] and [^{18}F]FEPPA ([^{18}F]**6**)[30] (Figure 1). These radioligands deliver higher TSPO-specific signals but suffer from sensitivity to the single nucleotide polymorphism (SNP) rs6971, which has an allelic frequency of about 30% in humans of European ancestry.[30−34] This SNP, which has no known clinical significance, is codominantly expressed, giving rise to high-affinity binders (HABs that have two high-affinity alleles), low-affinity binders (LABs that have two low affinity alleles), and mixed-affinity binders (MABs that have one low-

Received: June 20, 2014
Revised: August 14, 2014
Published: August 15, 2014

   dx.doi.org/10.1021/cn500138n | *ACS Chem. Neurosci.* 2014, 5, 963−971

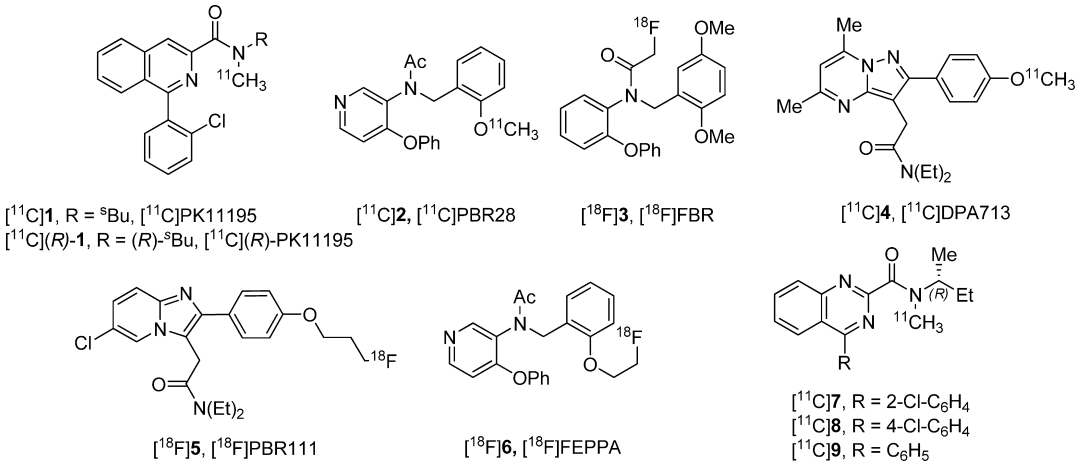

Figure 1. Structures of some known TSPO PET radioligands and of [11C]**7**−**9**.

Table 1. In Silico and in Vitro Properties of 1 and 7−9

				HAB K_i (nM)		LAB K_i (nM)		LAB K_i/HAB K_i		
Ligand	Rat K_i (nM)[a]	clogD	logD[b]	Leukocytes[c]	Cerebellum[d]	Leukocytes[c]	Cerebellum[d]	Leukocytes	Cerebellum	LipE[e]
1	9.3 ± 0.5	3.72	3.97 ± 0.18	4.06 ± 1.20	4.53 ± 2.08	3.94 ± 1.20	4.16 ± 0.89	0.97	0.92	4.37
7	3.1 ± 0.3	2.95	3.55 ± 0.02	1.26 ± 0.57	1.48 ± 0.18	1.65 ± 0.26	1.89 ± 0.33	1.3	1.3	5.28
8	2.7 ± 0.3	3.22	3.540 ± 0.005	0.91 ± 0.47	1.01 ± 0.35	2.20 ± 1.0	2.64 ± 0.88	2.4	2.6	5.46
9	3.0 ± 0.3	2.54	2.98 ± 0.01	3.99 ± 0.85	5.74 ± 0.77	10.1 ± 2.6	15.6 ± 1.9	2.5	2.7	5.26

[a]From ref 35. [b]Mean ± SD for n = 6. [c]Mean ± SD for leukocytes from 5 subjects, except 4 HAB subjects were used for **9**. [d]Mean ± SD for cerebellum from 4 subjects. [e]pK_i − logD for human cerebellum HAB.

and one high-affinity allele). The differential affinity of the two alleles can be large for some radioligands, for example, about 50-fold difference in affinity for [11C]**2**. Depending on the radioligand, LABs have such negligible uptake in brain that they must be excluded from PET study. In addition, HAB and MAB subjects must be genotyped to correct for the effect of genotype on binding. Therefore, an effective TSPO PET radioligand that is devoid of sensitivity to SNP rs6971 would be valuable.

Despite its other limitations, [11C](*R*)-**1** shows exceptionally low sensitivity to SNP rs697 in vitro,[33] although it may have some sensitivity in vivo.[23] We recently reported a series of 4-phenylquinazoline-2-carboxamides as TSPO ligands designed as azaisosteres of **1**.[35,36] A wide number of variously decorated derivatives were synthesized and biologically evaluated, most of which showed high TSPO binding affinity with K_i values in the nanomolar/subnanomolar range and with high selectivity toward the target protein. Specifically, three of these ligands (**7**−**9**) were considered to present attractive properties for PET radioligand development, including high TSPO affinity and moderate lipophilicity. Here we sought to prepare the three radioligands [11C]**7**−**9** (Figure 1) for evaluation of their abilities to image TSPO in monkey brain. In view of our findings of promising TSPO imaging characteristics for [11C]**7**−**9** in monkey, we also used assays with human leukocytes and postmortem human cerebellum to establish that their TSPO binding characteristics were promising for PET imaging of all TSPO genotypes.

RESULTS AND DISCUSSION

Our selection of the three 4-phenylquinazoline-2-carboxamides **7**−**9** for labeling with carbon-11 (β^+, $t_{1/2}$ = 20.4 min) and evaluation as possible PET radioligands for brain TSPO was initially guided by their high affinities toward TSPO and their computed moderate lipophilicities (clogD values) (Table 1), which are consistent with achieving adequate brain entry and low nonspecific binding.[37−40] In this regard, **7**−**9** favorably presented superior affinity and attenuated lipophilicity with respect to **1** (Table 1). Here we found that these three ligands were readily labeled with carbon-11 and showed high TSPO-specific PET signals in rhesus monkey brain. In addition, they were found to show low sensitivity to human TSPO genotype in vitro. Overall, [11C]**7**, in particular, merits evaluation in human subjects.

Radiochemistry. The three radioligands [11C]**7**−**9** were prepared rapidly by treating the respective *N*-desmethyl analogs **10**−**12** with [11C]methyl iodide in DMSO with potassium hydroxide as base (Figure 2). Each radioligand was purified by

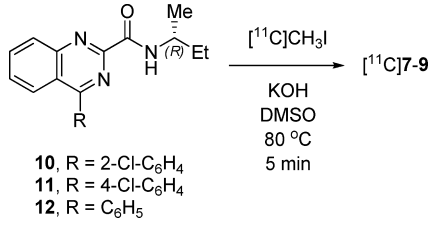

Figure 2. Labeling of **7**−**9** with carbon-11.

reverse phase HPLC and formulated for intravenous injection. HPLC analysis showed that each formulated radioligand was obtained in high radiochemical purity (>99%), in high specific radioactivity (typically >55 GBq/μmol at end of synthesis) (Table 2), and free of significant chemical contaminants as judged by the absence of major unknown absorbance peaks in HPLC analysis. Moreover, each formulated radioligand was radiochemically stable for at least 2 h. Adequate activities (>90 MBq) were readily obtained for PET imaging in monkey.

dx.doi.org/10.1021/cn500138n | ACS Chem. Neurosci. 2014, 5, 963−971

Table 2. Radiochemical Yields, Purities, and Specific Activities of [^{11}C]7−9

Radioligand	Decay-corrected radiochemical yield (%)	Radiochemical purity (%)	Specific radioactivity range at EOS[a] (GBq/μmol)
[^{11}C]**7**	17−29	100	72.2−203 (n = 4)
[^{11}C]**8**	23−28	100	79.6−226 (n = 4)
[^{11}C]**9**	18−27	100	53.7−329 (n = 6)

[a]End of synthesis.

Lipophilicity Measurements. Measured radioligand logD values were found, as expected, to be almost identical for the two chloro isomers [^{11}C]**7** and [^{11}C]**8**, namely ∼3.5, and appreciably higher than for the nonchloro compound [^{11}C]**9** (Table 1). As expected, all three quinazoline radioligands [^{11}C]**7**−**9** have lower lipophilicity than the counterpart isoquinoline **1** (logD, 3.97), which has one less ring nitrogen. Measured logD values are in fair agreement with our computed values, upon which the selection of **7**−**9** for further development as PET radioligands was made.

PET Imaging of [^{11}C]7−9 in Monkeys. The ability of radioligands [^{11}C]**7**−**9** to image brain TSPO was tested with PET in rhesus monkeys, first after radioligand injection at baseline, and second after preblocking TSPO with **1** (5 mg/kg, i.v.) at about 5 min before injection of radioligand. Summed PET images of monkey brain acquired after radioligand injection (Figure 3) displayed a high level of radioactivity, especially in the

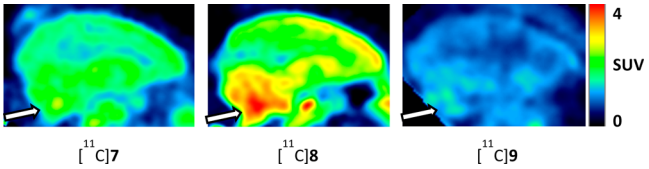

Figure 3. Sagittal summed PET images of brain after intravenous injection of the same monkey with [^{11}C]**7**−**9** under baseline conditions. Arrows point to the choroid plexus of the fourth ventricle.

choroid plexus of the fourth ventricle. High uptake was also seen in striatum and cerebellum, and to a lesser extent in cortical regions. Scans from the corresponding preblock experiments showed a very uniform and low distribution of radioactivity, consistent with the absence of radioligand specific binding to TSPO (data not shown).

At baseline, [^{11}C]**7**−**9** were estimated to have mean peak whole brain concentrations of 2.0, 2.3, and 1.8 SUV at about 23, 30, and 10 min (all, n = 2), respectively (Figure 4). This moderately high uptake is comparable to that achieved with other prominent TSPO radioligands, such as [^{11}C]**2**[24] and [^{18}F]**3**.[27] Subsequent washout of radioactivity from all TSPO-containing regions was slow, reducing to 86, 92, and 36% of the peak value at 60 min for [^{11}C]**7**−**9**, respectively (Figure 4). In TSPO preblock experiments, the kinetics of brain radioactivity was strikingly different. Peak brain radioactivity was much higher and earlier but declined much faster than at baseline to reach a low terminal level (Figure 4), thereby evidencing the TSPO receptor block in the brain. These data together indicate a high proportion of radioligand specific binding to brain TSPO in the baseline experiments.

Regional brain time-activity curves for each radioligand at baseline and at preblock showed the same shape as the whole brain curves, with the exception of the curve for the choroid plexus of the fourth ventricle for [^{11}C]**9** (Figure 5). The positional isomers, [^{11}C]**7** and [^{11}C]**8**, have very similar affinity and lipophilicity in vitro (Table 1) and gave very similar time-activity curves under each condition, although brain uptake was somewhat higher for [^{11}C]**8**. For each radioligand at baseline, peak radioactivities were highest in the choroid plexus of the fourth ventricle, followed by putamen, cerebellum, and all other examined regions (Figure 5). In the preblock experiment with each radioligand, regional time-activity curves were virtually superimposed, with the exception of the choroid plexus curve for [^{11}C]**9**, which remained higher than for other regions. These data evidence equal nonspecific binding for [^{11}C]**7** and [^{11}C]**8** in all regions and equal nonspecific binding for [^{11}C]**9** in all regions except the choroid plexus of the fourth ventricle (Figure 5).

In some paired baseline and preblock PET experiments, a metabolite-corrected arterial input function for unchanged radioligand was measured (see below) and used with Logan graphical analysis[41] to derive a measurement of radioligand binding in terms of total distribution volume, V_T.[42] Logan-V_T values for [^{11}C]**7**−**9** determined for direct comparison in cerebellum of a single monkey were found to be 11.3, 25.6, and 2.4 mL/cm^3 at baseline and 2.0, 3.3, and 1.4 mL/cm^3 at preblock, indicating 82, 87, and 42% TSPO specific binding at baseline, respectively (Table 3). V_S, the difference between baseline and preblock V_T, may be taken as a measure of specific binding. V_S values for [^{11}C]**7** and [^{11}C]**8** are 9.3 and 22.3 mL/cm^3, which are substantially higher than the V_S value (∼2 mL/cm^3) found[23] for [^{11}C](*R*)-**1**. V_S for [^{11}C]**9** is lower than that of [^{11}C](*R*)-**1**. These data do not take into account changes in brain exposure to radioligand due to changes in plasma free fraction between baseline and preblock conditions. After correction for measured free fraction changes in the same monkey (Table 4),

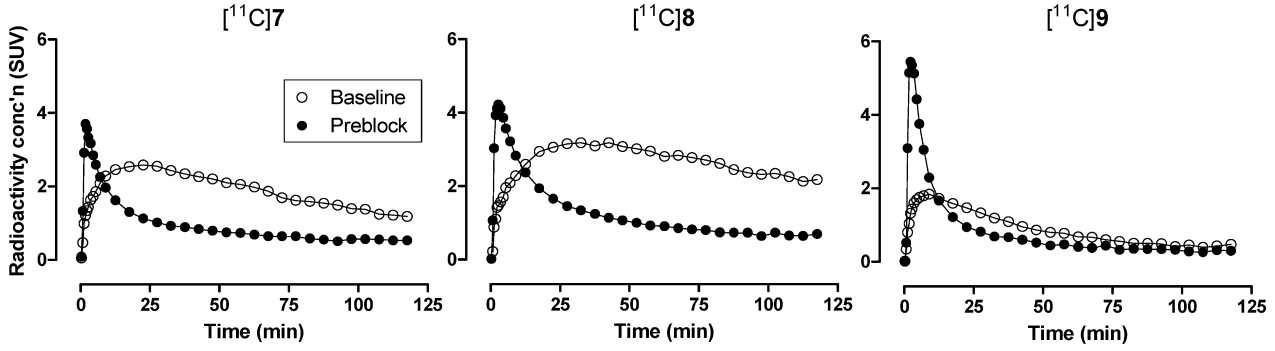

Figure 4. PET time-activity curves in whole rhesus monkey brain following intravenous injection of [^{11}C]**7**−**9** under baseline and TSPO-preblocked conditions. Data are from a single monkey.

dx.doi.org/10.1021/cn500138n | ACS Chem. Neurosci. 2014, 5, 963−971

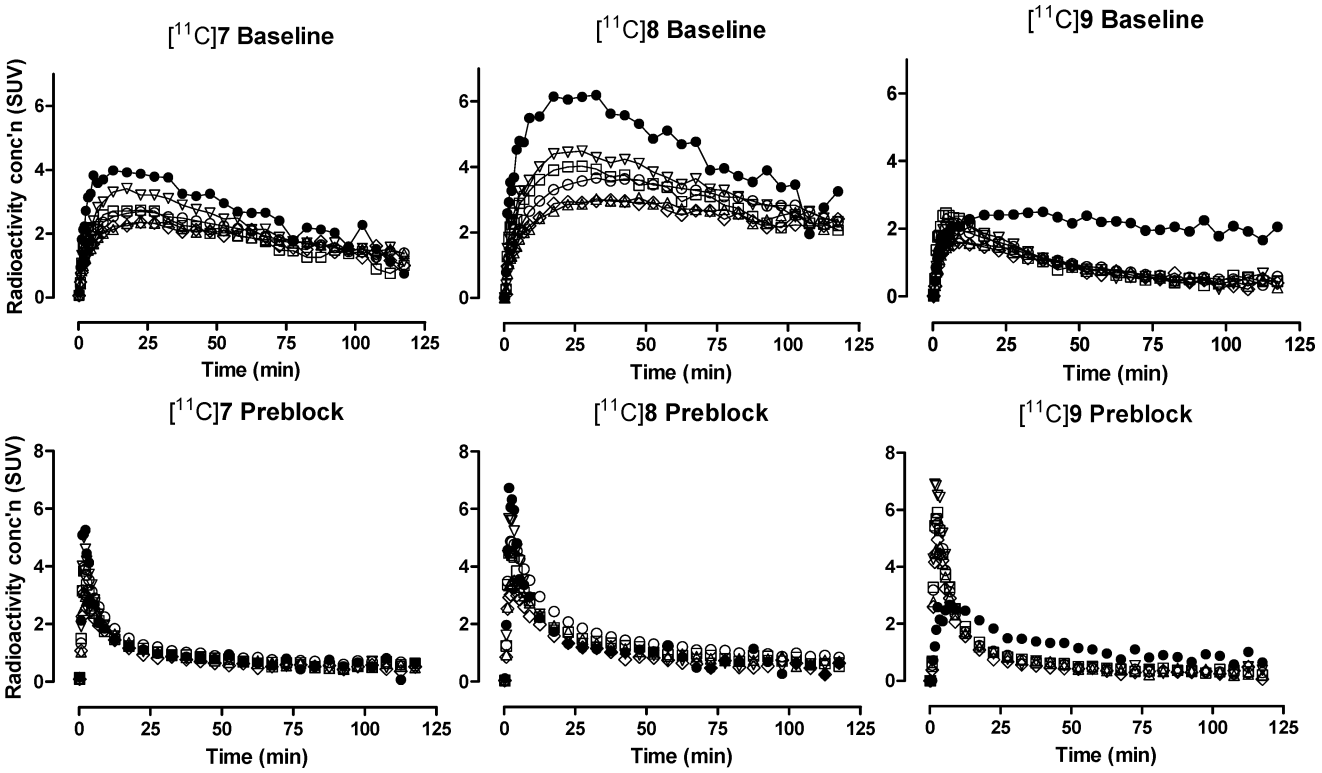

Figure 5. Time-activity curves in brain regions of the same monkey following intravenous injection of [^{11}C]**7**–**9** under baseline and TSPO-blocked conditions. Key: Anterior cingulate (△), cerebellum (□), choroid plexus of the fourth ventricle (●); hippocampus (◇), prefrontal cortex (○), and putamen (▽).

Table 3. Estimation of TSPO Specific Binding in Monkey Cerebellum from V_T at Baseline and under Preblock Conditions, with and without Correction for Plasma Free Fraction (f_P)[a]

Radioligand	V_T at baseline (mL/cm^3)	V_T at preblock (mL/cm^3)	Est of TSPO specific binding[b] (%)	V_T/f_P at baseline (mL/cm^3)	V_T/f_P at preblock (mL/cm^3)	Est of TSPO specific binding[c] (%)
[^{11}C]**7**	11.3	2.0	82	141	17.2	88
[^{11}C]**8**	25.6	3.3	87	533	60	89
[^{11}C]**9**	2.4	1.4	42	34.8	7.5	78

[a]All data are from the same monkey. [b]From V_T values. [c]From V_T/f_P values.

Table 4. Extraction Efficiencies and Retention Volumes of [^{11}C]7–9 and Their Radiometabolites in Reverse Phase HPLC Analysis and Time To Reach Radioligand as Half Plasma Activity and Plasma Free Fractions (f_P)[a]

		Retention volume (mL)					Time to reach radioligand as half plasma activity (min)		f_P[c]	
			Radiometabolite							
Radioligand	Extraction efficiency (%)[b]	Radioligand	A	B	C	D	Baseline	Preblock	Baseline	Preblock
[^{11}C]**7**	95.4 ± 4.0	9.5 ± 1.6	3.6 ± 1.2	4.8 ± 1.2	5.9 ± 1.2	7.2 ± 1.6	35.1	9.57	0.080 ± 0.003	0.116 ± 0.003
[^{11}C]**8**	94.7 ± 5.3	11.0 ± 1.2	4.0 ± 1.3	5.4 ± 1.1	7.0 ± 1.2	8.2 ± 1.2	69.3	13.9	0.048 ± 0.003	0.055 ± 0.005
[^{11}C]**9**	95.9 ± 2.8	8.8 ± 2.5	3.8 ± 1.2	5.1 ± 1.6	6.5 ± 1.9[d]		26.0	9.4	0.069 ± 0.004	0.186 ± 0.001

[a]All data are from the same monkey. [b]From plasma into acetonitrile; mean ± SD for n = 34. [c]Mean ± SD for n = 3. [d]C and D were not well resolved.

estimates of TSPO specific binding at baseline became 88, 89, and 78%, respectively (Table 3). Clearly, [^{11}C]**7** and [^{11}C]**8** have appreciably greater V_T/f_P values than [^{11}C]**9**. It was therefore of interest to assess the duration of PET data that needs to be acquired to obtain acceptably stable V_T values, which are often considered to be values that are sustained within 90% of the terminal value. Figure 6 shows the variation in cerebellar V_T's for [^{11}C]**7** and [^{11}C]**8** with respect to their estimation from increasing durations of PET data acquired immediately following radioligand administration. At baseline, both radioligands reach 90% of terminal values by about 70 min. Whereas the curve for [^{11}C]**7** appears to be almost stabilized by 120 min, that for [^{11}C]**8** appears still to be rising steadily. Therefore, on this basis, [^{11}C]**7**

dx.doi.org/10.1021/cn500138n | ACS Chem. Neurosci. 2014, 5, 963–971

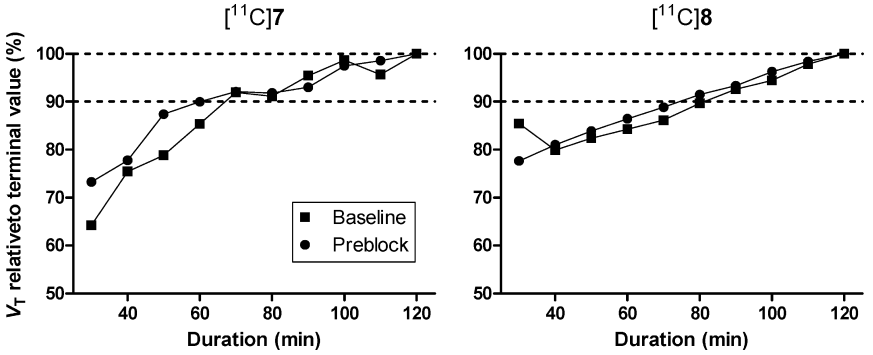

Figure 6. Time-stability of volumes of distribution estimated from Logan analysis of PET data in the cerebellum of the same monkey after administration of [^{11}C]7 and [^{11}C]**8** under baseline and TSPO preblock conditions. The *x*-axis is the duration of PET data acquired from the start of radioligand administration that was used to calculate V_T.

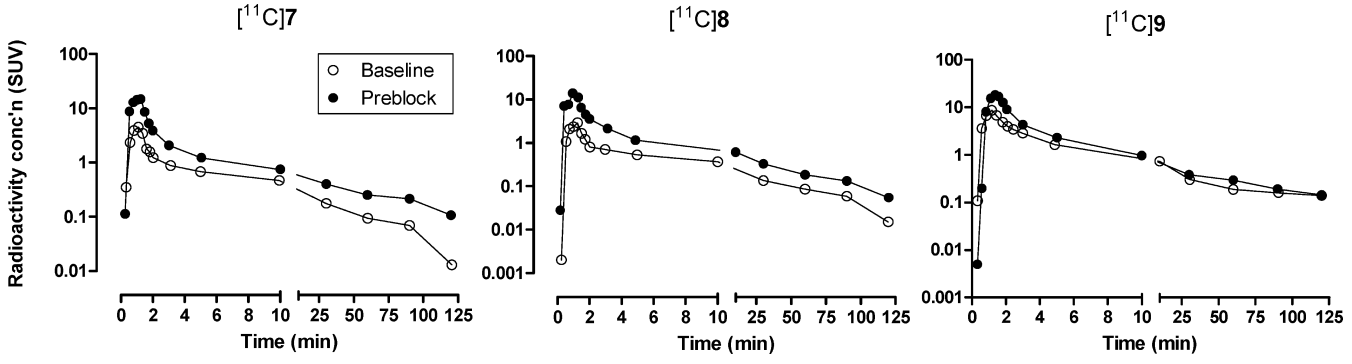

Figure 7. Time-courses of concentration of unmetabolized [^{11}C]**7**–**9** in plasma after intravenous injection into the same monkey under baseline and preblocked conditions.

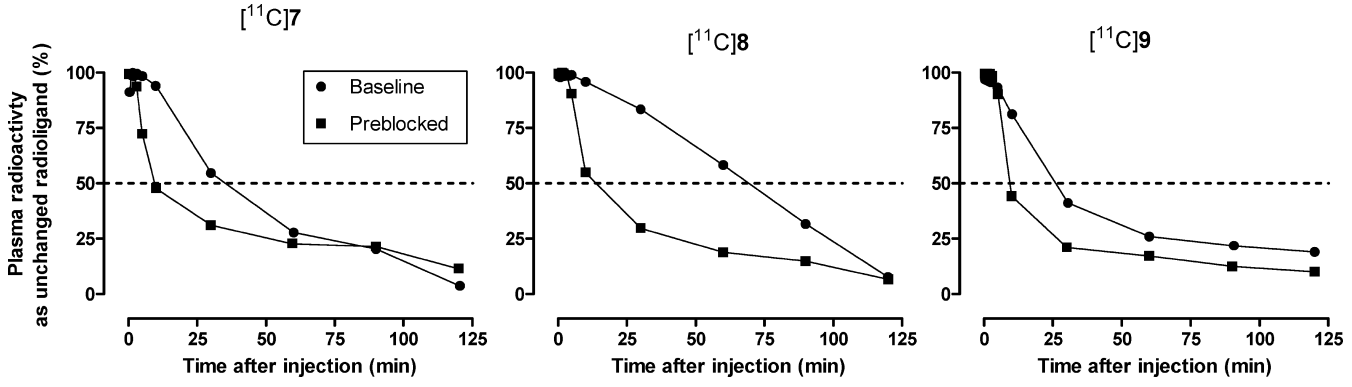

Figure 8. Time-courses of plasma radioactivity composition in terms of parent radioligand after i.v. administration of [^{11}C]**7**–**9** to the same monkey under baseline and TSPO preblock conditions. The dotted lines intersect the curves when radiometabolites become half the radioactivity in plasma.

appears to have more favorable kinetics for quantifying TSPO in monkey brain than [^{11}C]**8**.

Emergence of Radiometabolites of [^{11}C]7–9 in Monkey Plasma in Vivo. Generally, PET radioligands are appreciably metabolized over the short time-span of a subject scanning session. As seen above, quantitative analysis of radioligand kinetics to derive output measures such as V_T may require determination of the amount of unmetabolized radioligand in plasma over the full duration of a scanning session. PET radioligands that produce brain-penetrant radiometabolites are often difficult to quantify.[37,42] For these reasons, we assessed the emergence of radiometabolites in monkey plasma following intravenous administration of [^{11}C]**7**–**9**.

The three radioligands were stable in whole blood and plasma in vitro. Recoveries of radioactivity from monkey plasma into acetonitrile for reverse phase HPLC analysis exceeded 94% (Table 4). After administration of any of the three radioligands [^{11}C]**7**–**9** into monkey, the percentage of radioactivity in plasma represented by unchanged radioligand decreased rapidly, and much more so in preblock experiments than in baseline experiments with the same radioligand (Figure 7). Thus, for [^{11}C]**7**–**9**, plasma radioactivity became composed equally of radiometabolites and parent radioligand at 35.1, 69.3, and 26.0 min in baseline experiments and at 9.57, 13.9, and 9.40 min in TSPO-preblock experiments in the same monkey, respectively (Figure 8, Table 4). Moreover, the normalized concentrations of unchanged radioligand in plasma (SUV) were much higher in the

dx.doi.org/10.1021/cn500138n | ACS Chem. Neurosci. 2014, 5, 963–971

preblock experiments than in the coupled baseline experiments (Figure 7). Such differences have also been seen for other prominent TSPO radioligands.[24,27] The lower concentration of unchanged radioligand in plasma in baseline experiments may be ascribed to a depletion through binding to abundant TSPO receptors in peripheral organs that does not occur under TSPO blocking conditions. The greater plasma availability of unchanged radioligand under preblock conditions likely explains the faster appearance of radiometabolites.

For each radioligand, analyses of plasma from monkeys studied at baseline revealed four radiometabolites, all with shorter retention times than the parent radioligand (Table 4). The identities of the radiometabolites are currently unknown, as are their abilities to penetrate the blood-brain barrier.

Radioligand Plasma Free Fraction. Among other factors, the radioligand plasma free fraction (f_P) has a strong influence on the ability of a radioligand to enter the brain. Generally, it is assumed that only free radioligand in plasma can enter the brain. The plasma free fractions of [^{11}C]**7**–**9** in blood sampled from the same monkey during baseline and preblock PET scans are shown in Table 4. These are moderately low at baseline, ranging from 0.048 for [^{11}C]**8** to 0.080 for [^{11}C]**7**, in accord with their moderate ligand lipophilicities (measured logD values),[43] but substantially higher than that of the more lipophilic [^{11}C](*R*)-**1** (f_P, 0.0207). Plasma free fractions were much higher under preblock conditions than under baseline conditions, especially for [^{11}C]**9**.

Ligand Affinity to TSPO in Human Leukocytes and Human Cerebellum in Vitro. As assessed in human leukocytes in vitro, ligands **7**–**9**, respectively, showed high affinities for human HAB TSPO (K_i = 1.26, 0.910, and 3.99 nM; *cf.* K_i = 4.06 nM for **1**) and low ratios (1.3, 2.4, and 2.5; *cf.* 0.97 for **1**) of LAB to HAB TSPO affinity (Table 1). An almost identical pattern of binding affinities and of LAB to HAB binding affinity ratios emerged from assays on postmortem human cerebellum (Table 1). Although the cerebellum assays were conducted at 37 °C and the leukocyte assays at room temperature, K_i values were very similar. Again, among **7**–**9**, ligand **7** showed the lowest ratio (1.3) of LAB to HAB TSPO affinity. We estimate that if a similar binding affinity ratio applied in PET studies of human subjects of Caucasian ancestry in vivo, the likely error in estimating binding potential without genotype correction would be about 7% (see Supporting Information).

For ligands **7**–**9**, the ratios of HAB TSPO affinity in cerebellum to measured lipophilicity (logD), as captured in the LipE[44] scores (5.28, 5.46, and 5.26, respectively), are appreciably superior to that of **1** (4.37) (Table 1). The high LipE scores for [^{11}C]**7**–**9** are consistent with the high proportions of TSPO-specific binding found in the monkey brain imaging (Table 3).

In summary, among a wide series of 4-phenylquinazoline-2-carboxamide azaisosters of **1**, recently reported as potent TSPO ligands,[35,36] three derivatives (**7**–**9**) were selected for PET radioligand development in view of their high TSPO affinity and moderate lipophilicity. [^{11}C]**7**–**9** were each easily prepared and readily entered monkey brain to give a high proportion of specific binding to brain TSPO. As a PET radioligand in monkey, unlike [^{11}C]**8** and [^{11}C]**9**, [^{11}C]**7** has an array of favorable properties which are as good as or better than those of [^{11}C](*R*)-**1**.[23] These include lower lipophilicity, higher free fraction, higher LipE score, higher HAB TSPO affinity, similar very low genotype sensitivity in vitro, higher TSPO-specific signal, higher proportion of TSPO-specific binding, and better amenability to quantification without highly problematic radiometabolites.

In conclusion, [^{11}C]**7** warrants further evaluation in human subjects and in particular to determine whether the very low sensitivity seen in vitro is reflected in vivo. We have previously found that [^{11}C]**1** has significant in vivo sensitivity in peripheral organs between LABs and a combined group of HABs and MABs.[23] Thus, a discrepancy between in vitro and in vivo sensitivity may also exist for [^{11}C]**7**. Imaging with [^{11}C]**7** both in brain and in peripheral organs of humans will be the critical test of its sensitivity to rs6971 and of its potential utility as a biomarker of inflammatory disorders.

METHODS

Materials and Methods. All reagents were obtained from commercial sources (Sigma-Aldrich; St Louis, MO). All solvents were analytical grade. Racemic [^{3}H]**1** (specific activity, 3.14 GBq/μmol) was purchased from PerkinElmer Life Sciences (Waltham, MA). Human blood samples were obtained under approval from the Intramural Review Board of the National Institutes of Health.

γ-Radioactivity from ^{11}C was measured using a calibrated dose calibrator (Atomlab 300; Biodex Medical Systems, Inc.; Shirley, NY). Radioactivity measurements were corrected for physical decay. All radiochemistry was performed in lead-shielded hot-cells for personnel protection from radiation.

Ligands **7**–**9** and their *N*-desmethyl analogs **10**–**12** were prepared as described previously.[35]

Assay of Ligands for Affinity to Human Leukocyte TSPO Genotypes. Ligands **7**–**9** were subjected to receptor binding assays at room temperature in human leukocyte homogenates[12] with [^{3}H]**1** as radioligand to characterize ligand binding sensitivities to TSPO polymorphism. Blood samples were obtained under National Institutes of Health IRB approval and after obtaining consent from study participants. K_i values were measured in triplicate in five high-affinity (HABs) and five low-affinity (LABs) binding tissues whose affinity status had been predetermined. As a control in each assay, a self-displacement assay was used to calculate the K_D of **1**. A mean K_D value of 4.7 nM[23] was then used as the dissociation constant for **1** to calculate ligand K_i.[45] Nonlinear regression curve-fitting software (GraphPad Prism 5; GraphPad Software; San Diego, CA) was used to fit data to a one-site model to provide ligand K_i values.

Assay of Ligands for Affinity to Human Cerebellum TSPO Genotypes. Ligands **7**–**9** were also subjected to receptor binding assays in postmortem healthy human cerebellum homogenates with [^{3}H]**1** as radioligand to characterize ligand binding sensitivities to the TSPO polymorphism. K_i values were measured in triplicate in four high-affinity (HABs) and four low-affinity (LABs) cerebellum tissues whose affinity status had been predetermined by genotype. Binding assays were performed in a similar manner to those in leukocytes, except assays were incubated for 1 h at 37 °C. As a control in each assay, a self-displacement assay was used to calculate the K_D of **1**. A mean K_D value of 4.35 nM was then used as the dissociation constant for **1** to calculate ligand K_i.[45] Nonlinear regression curve-fitting software (GraphPad Prism 5; GraphPad Software; San Diego, CA) was used to fit data to a one-site model to provide ligand K_i values.

Production of NCA [^{11}C]Carbon Dioxide. No-carrier-added (NCA) [^{11}C]carbon dioxide (~85 GBq) was produced with a PETtrace cyclotron (GE Medical Systems; Milwaukee, WI) according to the ^{14}N(p,α)^{11}C reaction[46] by irradiation of nitrogen gas (initial pressure 160 psi; 75 mL volume) containing 1% oxygen with a proton beam (16.5 MeV, 45 μA) for 40 min.

Radiochemistry. All radiochemistry was performed in an upgraded[47] PLC-controlled apparatus based on an original semirobotic Synthia instrument[48] (Synthia AB; Uppsala, Sweden), housed within a lead-shielded hot-cell for personnel protection.

Production of NCA [^{11}C]Methyl Iodide. NCA [^{11}C]methyl iodide was produced from NCA [^{11}C]carbon dioxide via reduction to [^{11}C]methane and then vapor phase iodination.[49] Thus, at the end of the proton irradiation, [^{11}C]carbon dioxide was delivered to a PETtrace MeI Process Module (GE Medical Systems; Severna Park, MD) through

stainless tubing (OD 1/8 in, ID 1/16 in) over 2 min and trapped on molecular sieve (13X) and reduced to [^{11}C]methane over nickel at 360 °C. The [^{11}C]methane was recirculated over iodine at 720 °C to generate [^{11}C]methyl iodide, which was trapped on Porapak Q held in the recirculation path.

Radiosynthesis of [^{11}C]7. [^{11}C]Iodomethane in carrier helium (15 mL/min) was bubbled into a 1 mL V-vial containing the secondary amide precursor **10** (0.6 mg) and KOH (1.2 mg) in DMSO (0.4 mL). When the radioactivity in the vial had maximized, the reaction mixture was sealed and heated at 80 °C for 5 min and then diluted with water. The reaction mixture was then injected onto an XTerra RP18 column (10 μm; 7.8 mm × 300 mm; Waters Corp.; Columbia, MD) eluted at 8 mL/min with MeCN: 1 mM aq. NH_4OH (37:63 v/v). [^{11}C]7 (t_R, ca. 15.3 min) was collected in a 50-mL flask. This solution was concentrated to dryness by rotary evaporation under reduced pressure and heat (80 °C). The radioactive residue was formulated in sterile physiological saline (0.9% w/v; 10 mL) containing ethanol (5% v/v), and filtered through a sterile filter (0.2 μm pore size, Millex-MP, 25 mm; Millipore, Billerica, MA) into a sterile, pyrogen-free dose vial.

Formulated [^{11}C]7 (t_R, ca. 7.3 min) was analyzed for radiochemical and chemical purity on an Xterra RP18 column (5 μm, 4.6 mm × 250 mm; Waters Corp.) eluted with MeCN: 10 mM aq. NH_4OH (56:44 v/v) at 1.5 mL/min with eluate monitored for radioactivity (pin diode detector; Bioscan Inc.; Washington, DC) and absorbance at 235 nm. A sample was injected onto HPLC alone, and in a subsequent analysis along with authentic **7** to check for coelution. Product identity was further confirmed by LC-MS/MS of associated carrier on a Finnigan LCQ DECA instrument (ThermoFisher Scientific; Rockville, MD).

Radiosynthesis of [^{11}C]8. [^{11}C]**8** was prepared as described for [^{11}C]**7**, except that the reaction mixture consisted of secondary amide precursor **11** (1.0 mg) and KOH (1.0 mg) in DMSO (0.4 mL), and the HPLC separation was conducted with a mobile phase of MeCN: 10 mM aq. NH_4OH (41:59, v/v) ([^{11}C]**8**; t_R, ca. 14.4 min).

[^{11}C]**8** (t_R, ca. 6.8 min) was analyzed as described for [^{11}C]**7**, except that the HPLC mobile phase was MeCN: 1 mM aq. NH_4OH (58:42 v/v).

Radiosynthesis of [^{11}C]9. [^{11}C]**9** was prepared as described for [^{11}C]**7**, except that the reaction mixture consisted of secondary amide precursor **12** (1.0 mg) and KOH (3.0 mg) in DMSO (0.4 mL), and that the HPLC separation was conducted with a mobile phase of MeCN: 10 mM aq. NH_4OH (38:62, v/v) ([^{11}C]**9**; t_R, ca. 10.4 min).

[^{11}C]**9** was analyzed as described for [^{11}C]**7**, except that the mobile phase was MeCN:10 mM aq. NH_4OH (55:45 v/v) and the absorbance detector was set to read at 254 nm ([^{11}C]**9**; t_R, ca. 6.0 min).

Computation of cLogD. cLogD (at pH 7.4) values for **7**–**9** were computed with Pallas for Windows software version 3.8 in default mode (CompuDrug International; Bal Harbor, FL).

Measurement of LogD. LogD (at pH 7.4) was measured on each radioligand by partition between *n*-octanol and sodium phosphate buffer (pH 7.4) at room temperature, as described in detail previously.[43]

PET Experiments with [^{11}C]7–9 in Monkeys. PET scans were performed in six male rhesus (*Macaca mulatta*) monkeys (8.7–11.1 kg). All animals were handled in accordance with the *Guide for the Care and Use of Laboratory Animals*[50] and the National Institute of Health Animal Care and Use Committee. For each scanning session, the subject monkey was immobilized with ketamine (10 mg/kg; i.m.) and maintained under anesthesia with 1–3% isoflurane and 98.4% oxygen. Head position was fixed with a stereotactic frame. An intravenous perfusion line, filled with saline (0.9% w/v), was used for bolus injection of radioligand of 99.9% radiochemical purity. Dynamic PET images of brain radioactivity were obtained for up to 120 min on a microPET Focus F220 scanner (Siemens Medical Solutions Inc.; Knoxville, TN), with frame durations ranging from 30 s to 5 min. All PET images were corrected for attenuation and scatter.

Baseline scans were performed with each radioligand in two (for [^{11}C]**7** and [^{11}C]**8**) or three (for [^{11}C]**9**) monkeys, one of which, weighing between 10.7 and 11.1 kg, was used in separate sessions for all three radioligands. Radioligands (165–217 MBq) were administered with low carrier mass doses of 1.27–5.4 nmol/kg. Each baseline scan was paired with a TSPO preblock scan at least 3 h later in the same monkey in which the TSPO ligand **1** (5 mg/kg, i.v.) was administered at 15 min before a second injection of the same radioligand (175–253 MBq; carrier dose 3.3–6.7 nmol/kg).

Image Analysis. PET Images were reconstructed using Fourier rebinning plus two-dimensional filtered back-projection. An averaged PET image was created by averaging all frames of PET images. The averaged PET image was normalized to a standardized monkey MRI template using SPM8 (Wellcome Trust Centre; London, UK), and the transformation parameters were applied to the normalization of the individual PET frames. A predefined atlas of volumes of interest was then applied to the normalized dynamic scan to obtain decay-corrected time-activity curves for several brain regions, namely amygdala, anterior cingulate, basofrontal cortex, caudate, cerebellum, hippocampus, hypothalamus, insula, lateral temporal cortex, medial temporal cortex, midbrain, parietal cortex, occipital cortex, pons, posterior cingulate, prefrontal cortex, putamen, temporal cortex, and thalamus. The choroid plexus of the fourth ventricle was not defined in the atlas and was manually defined for each monkey. Regional radioactivity levels were normalized for injected dose and monkey weight and expressed as a standardized uptake value (SUV):

$$\mathrm{SUV} = [(\%\text{injected dose per g tissue}) \times \text{body weight in g}]/100.$$

PET Data Analysis. Total distribution volumes (V_T)[42] were estimated for different regions by Logan graphical analysis[41] using the PET brain time-activity curves and the measured metabolite-corrected arterial input function. The temporal stabilities of V_T in cerebellum in the baseline and preblock experiments were assessed by estimating V_T from progressively time-truncated data sets. The PET data analysis was performed using PMOD (PMOD Technologies Ltd.; Zurich, Switzerland).

Stability of [^{11}C]7–9 in Buffer and in Monkey Whole Blood and Plasma in Vitro. The stability of each formulated radioligand to incubation in sodium phosphate buffer (0.15 M, pH 7.4) for 2 h at room temperature was assessed by reverse phase radio-HPLC analysis. Each formulated radioligand (110–150 kBq; ~5 μL) was also incubated for 45 min at room temperature in either whole monkey blood or plasma (0.5 mL). A sample (0.3 mL) was removed from whole blood and added to water (0.4 mL) to lyse blood cells. Then the plasma (0.35 mL) or lysed cells were added to acetonitrile (0.8 mL), and centrifuged. Then the supernatant liquid was analyzed by reverse phase radio-HPLC on a Novapak C18 column (4 μm; 8 × 100 mm; Waters Corp.) eluted at 2.5 mL/min with MeOH/H_2O/Et_2O (75:25:0.1 by vol.).

Plasma Protein Binding of [^{11}C]7–9.[51] Each radioligand was added to pooled human plasma, placed at the top of an "Amicon" Centrifree filter unit (200 μL/unit) and filtered by ultracentrifugation at 5000 × *g*. Then all components of filter units were counted for radioactivity to allow calculation of radioligand plasma protein binding (f_P).

Emergence of Radiometabolites of [^{11}C]7–9 in Monkey Plasma In Vivo. During a baseline and a following preblock PET scan with each radioligand, blood samples were drawn periodically from the monkey femoral artery and collected in heparin-treated Vacutainer tubes. The samples were centrifuged and the plasma separated. A sample of plasma (0.45 mL) was mixed with acetonitrile (0.72 mL) and centrifuged. The supernatant liquid was analyzed with radio-HPLC on a Novapak C18 column (4 μm; 8 × 100 mm; Waters Corp.) eluted with MeOH/H_2O/Et_2O (75:25:0.1 by vol.). Time-courses for percentages of radioactivity in plasma represented by unchanged radioligand and its radiometabolites were then calculated.

■ ASSOCIATED CONTENT

Supporting Information

Binding curves from ligand assays on leukocytes and human cerebellar tissue, and estimation of binding potential error in human for [^{11}C]**7**, without genotype correction. This material is available free of charge via the Internet at http://pubs.acs.org/.

AUTHOR INFORMATION

Corresponding Author

*Tel.: +3015945986. Fax: +3014805112. E-mail: pikev@mail.nih.gov.

Author Contributions

S.T., C.M., F.D.S., R.B.I., and V.W.P. conceived the project. P.Z.-F., S.S.Z., M.F., K.J. J., R.B.I., and V.W.P. designed the experiments. P.Z.-F., Y.Z ., K.J. J., R.L.G., S.S.Z., and M.F. performed the experiments. G.S., S.C., S.T., C.M., and F.D.S. contributed ligands and precursors. P.Z.-F., K.J.J., S.S.Z., M.F., R.B.I., and V.W.P. performed data analyses. P.Z.-F., Y.Z., S.S.Z, K.J.J., C.M., F.D.S., and V.W.P. wrote the manuscript. All authors edited and approved the final version of the manuscript.

Funding

This study was supported by the Intramural Research Program of the National Institutes of Health (NIH), specifically the National Institute of Mental Health (NIMH), and MIUR (PRIN 2009, Futuro in Ricerca 2010, PRIN 2011).

Notes

The authors declare the following competing financial interest(s): Drs. Pike, Innis, Zhang, Zoghbi, Castellano, Da Settimo, Martini, and Taliani are named as applicants on a U.S. patent appication with regard to the subject of this publication.

ACKNOWLEDGMENTS

We thank PMOD Technologies Ltd. (Zurich, Switzerland), for providing PMOD software to analyze PET data. We also thank Mr. David T. Clark for effective assistance with experiments in plasma.

ABBREVIATIONS

HAB, high-affinity binder; LAB, low-affinity binder; MAB, mixed-affinity binder; NCA, no-carrier-added; PET, positron emission tomography; TSPO, translocator protein (18 kDa)

REFERENCES

(1) Papadopoulos, V., Baraldi, M., Guilarte, T. R., Knudsen, T. B., Lacapere, J. J., Lindemann, P., Norenberg, M. D., Nutt, D., Weizman, A., Zhang, M., and Gavish, M. (2006) Translocator protein (18 kDa): new nomenclature for the peripheral-type benzodiazepine receptor based on its structure and molecular function. *Trends Pharmacol. Sci. 27*, 402−409.

(2) Doble, A., Malgouris, C., Daniel, M., Daniel, N., Imbault, F., Basbaum, A., Uzan, A., Guérémy, C., and Le Fur, G. (1987) Labelling of peripheral-type benzodiazepine binding sites in human brain with [^{3}H]PK 11195: anatomical and subcellular distribution. *Brain Res. Bull. 18*, 49−61.

(3) Casellas, P., Galiegue, S., and Basile, A. S. (2002) Peripheral benzodiazepine receptors and mitochondrial function. *Neurochem. Int. 40*, 475−486.

(4) Papadopoulos, V., Lecanu, L., Brown, R. C., Han, Z., and Yao, Z.-X. (2006) Peripheral-type benzodiazepine receptor in neurosteroid biosynthesis, neuropathology and neurological disorders. *Neuroscience 138*, 749−756.

(5) Rone, M. B., Ran, J., and Papadopoulos, V. (2009) Cholesterol transport in steroid biosynthesis: role of protein-protein interactions and implications in disease states. *Biochim. Biophys. Acta 1791*, 646−658.

(6) Veenman, L., and Gavish, M. (2000) Peripheral benzodiazepine receptors: their implication in brain disease. *Drug Dev. Res. 50*, 355−370.

(7) Cagnin, A., Brooks, D. J., Kennedy, A. M., Gunn, R. N., Myers, R., Turkheimer, F. E., Jones, T., and Banati, R. B. (2001) In-vivo measurement of activated microglia in dementia. *Lancet 358*, 461−467.

(8) Ouchi, Y., Yoshikawa, E., Sekine, Y., Futatsubashi, M., Kanno, T., Ogusu, T., and Torizuka, T. (2005) Microglial activation and dopamine terminal loss in early Parkinson's disease. *Ann. Neurol. 57*, 168−175.

(9) Debruyne, J. C., Versijpt, J., Van Laere, K. J., De Vos, F., Keppens, J., Strijckmans, K., Achten, E., Slegers, G., Dierckx, R. A., Korf, J., and De Reuck, J. L. (2003) PET visualization of microglia in multiple sclerosis patients using [^{11}C]PK11195. *Eur. J. Neurol. 10*, 257−264.

(10) Chelli, B., Pini, S., Abelli, M., Cardini, A., Lari, L., Muti, M., Gesi, C., Cassano, G. B., Lucacchini, A., and Martini, C. (2008) Platelet 18 kDa translocator protein density is reduced in depressed patients with adult separation anxiety. *Eur. Neuropsychopharmacol. 18*, 249−254.

(11) Dell'Osso, L., Da Pozzo, E., Carmassi, C., Trincavelli, M. L., Ciapparelli, A., and Martini, C. (2010) Lifetime manic-hypomanic symptoms in post-traumatic stress disorder: relationship with the 18 kDa mitochondrial translocator protein density. *Psychiatry Res. 177*, 139−143.

(12) Kreisl, W. C., Lyoo, C. H., McGwier, M., Snow, J., Jenko, K. J., Kimura, N., Corona, W., Morse, C. L., Zoghbi, S. S., Pike, V. W., McMahon, F. J., Turner, R. S., Innis, R. B., and Biomarkers Consortium PET Radioligand Project Team. (2013) *In vivo* radioligand binding to translocator protein correlates with severity of Alzheimer's disease. *Brain 136*, 2228−2238.

(13) Benavides, J., Fage, D., Carter, C., and Scatton, B. (1987) Peripheral type benzodiazepine binding sites are a sensitive indirect index of neuronal damage. *Brain Res. 421*, 167−172.

(14) Chen, M.-K., and Guilarte, T. R. (2008) Translocator protein 18 kDa (TSPO): molecular sensor of brain injury and repair. *Pharmacol. Ther. 118*, 1−17.

(15) Chaveau, F., Boutin, H., Van Camp, N., Dollè, F., and Tavitian, B. (2008) Nuclear imaging of neuroinflammation: a comprehensive review of [^{11}C]PK11195 challengers. *Eur. J. Nucl. Med. Mol. Imaging 35*, 2304−2319.

(16) Dollè, F., Luus, C., Reynolds, A., and Kassiou, M. (2009) Radiolabelled molecules for imaging the translocator protein (18 kDa) using positron emission tomography. *Curr. Med. Chem. 16*, 2899−2923.

(17) Schweitzer, P. J., Fallon, B. A., Mann, J. J., and Kumar, J. S. D. (2010) PET tracers for the peripheral benzodiazepine receptor and uses thereof. *Drug Discovery Today 15*, 933−942.

(18) Venneti, S., Lopresti, B. J., and Wiley, C. A. (2006) The peripheral benzodiazepine receptor (translocator protein 18 kDa) in microglia: from pathology to imaging. *Prog. Neurobiol. 80*, 308−322.

(19) Camsonne, R., Moulin, M. A., Crouzel, C., Syrota, A., Maziere, M., and Comar, D. (1986) ^{11}C-Labeling of PK 11195 and visualization of peripheral receptors of benzodiazepines by positron emission tomography. *J. Pharmacologie 17*, 383.

(20) Petit-Taboué, M. C., Baron, J. C., Barré, L., Travere, J. M., Speckel, D., Camsonne, R., and MacKenzie, E. T. (1991) Brain kinetics and specific binding of [^{11}C]PK11195 to ω_3 sites in baboon. *Eur. J. Pharmacol. 200*, 347−351.

(21) Shah, F., Hume, S. P., Pike, V. W., Ashworth, S., and McDermott, J. (1994) Synthesis of the enantiomers of [*N-methyl*-^{11}C]PK 11195 and comparison of their behaviours as radioligands for PK binding sites in rats. *Nucl. Med. Biol. 21*, 573−581.

(22) Banati, R. B., Goerres, G. W., Myers, R., Gunn, R. N., Turkheimer, F. E., Kreutzberg, G. W., Brooks, D. J., Jones, T., and Duncan, J. S. (1999) [^{11}C](*R*)-PK11195 positron emission tomography imaging of activated microglia in vivo in Rasmussen's encephalitis. *Neurology 53*, 2199−2203.

(23) Kreisl, W. C., Fujita, M., Fujimura, Y., Kimura, N., Jenko, K. J., Kannan, P., Hong, J., Morse, C. L., Zoghbi, S. S., Gladding, R. L., Jacobson, S., Oh, U., Pike, V. W., and Innis, R. B. (2010) Comparison of [^{11}C](*R*)-PK 11195 and [^{11}C]PBR28, two radioligands for translocator protein (18 kDa) in human and monkey: implications for positron emission tomographic imaging of this inflammation biomarker. *NeuroImage 49*, 2924−2932.

(24) Briard, E., Zoghbi, S. S., Imaizumi, M., Gourley, J. P., Shetty, H. U., Hong, J., Cropley, V., Fujita, M., Innis, R. B., and Pike, V. W. (2008) Synthesis and evaluation in monkey of two sensitive ^{11}C-labeled

aryloxyanilide ligands for imaging brain peripheral benzodiazepine receptors in vivo. *J. Med. Chem. 51*, 17−30.
(25) Imaizumi, M., Briard, E., Zoghbi, S. S., Gourley, J. P., Hong, J., Fujimura, Y., Pike, V. W., Innis, R. B., and Fujita, M. (2008) Brain and whole-body imaging in nonhuman primates of [^{11}C]PBR28, a promising PET radioligand for peripheral benzodiazepine receptors. *NeuroImage 39*, 1289−1298.
(26) Fujita, M., Imaizumi, M., Zoghbi, S. S., Fujimura, Y., Farris, A. G., Suhara, T., Hong, J., Pike, V. W., and Innis, R. B. (2008) Kinetic analysis in healthy humans of a novel positron emission tomography radioligand to image the peripheral benzodiazepine receptor, a potential biomarker for inflammation. *NeuroImage 40*, 43−52.
(27) Briard, E., Zoghbi, S. S., Siméon, F., Imaizumi, M., Gourley, J. P., Shetty, H. U., Lu, S.-Y., Fujita, M., Innis, R. B., and Pike, V. W. (2009) Single-step high-yield radiosynthesis and evaluation of a selective ^{18}F-labeled ligand for imaging brain peripheral benzodiazepine receptors with PET. *J. Med. Chem. 52*, 688−699.
(28) Endres, C. J., Pomper, M. G., James, M., Uzuner, O., Hammoud, D. A., Watkins, C. C., Reynolds, A., Hilton, J., Dannals, R. F., and Kassiou, M. (2009) Initial evaluation of [^{11}C]DPA-713, a novel TSPO PET ligand, in humans. *J. Nucl. Med. 50*, 1276−1282.
(29) Guo, Q., Colasanti, A., Owen, D. R., Onega, M., Kamalakaran, A., Bennacef, I., Matthews, P. M., Rabiner, E. A., Turkheimer, F. E., and Gunn, R. N. (2013) Quantification of the specific translocator protein signal of ^{18}F-PBR111 in healthy humans: a genetic polymorphism effect on in vivo binding. *J. Nucl. Med. 54*, 1915−1923.
(30) Mizrahi, R., Rusjan, P. M., Kennedy, J., Pollock, B., Mulsant, B., Suridjan, I., De Luca, V., Wilson, A. A., and Houle, S. (2012) Translocator protein (18 kDa) polymorphism (rs6971) explains *in-vivo* brain binding affinity of the PET radioligand [^{18}F]-FEPPA. *J. Cereb. Blood Flow Metab. 32*, 968−972.
(31) Owen, D. R., Howell, O. W., Tang, S.-P., Wells, L. A., Bennacef, I., Bergstrom, M., Gunn, R. N., Rabiner, E. A., Wilkins, M. R., Reynolds, R., Matthews, P. M., and Parker, C. A. (2010) Two binding sites for [^{3}H]PBR28 in human brain: implications for TSPO PET imaging of neuroinflammation. *J. Cerebr. Blood Flow Metab. 30*, 1608−1618.
(32) Kreisl, W. C., Jenko, K. J., Hines, C. S., Lyoo, C. H., Corona, W., Morse, C. L., Zoghbi, S. S., Hyde, T., Kleinman, J. E., Pike, V. W., McMahon, F. J., and Innis, R. B. (2013) A genetic polymorphism for translocator protein 18 kDa affects both in vitro and in vivo radioligand binding in human brain to this putative biomarker of neuroinflammation. *J. Cerebr. Blood Flow Metab. 33*, 53−58.
(33) Owen, D. R. J., Gunn, R. N., Rabiner, E. A., Bennacef, I., Fujita, M., Kreisl, W. C., Innis, R. B., Pike, V. W., Reynolds, R., Matthews, P. M., and Parker, C. A. (2011) Mixed-affinity binding in humans with 18-kDa translocator protein ligands. *J. Nucl. Med. 52*, 24−32.
(34) Owen, D. R., Yeo, A. J., Gunn, R. N., Song, K., Wadsworth, G., Lewis, A., Rhodes, C., Pulford, D. J., Bennacef, I., Parker, C. A., StJean, P. L., Cardon, L. R., Mooser, V. E., Matthews, P. M., Rabiner, E. A., and Rubio, J. P. (2012) An 18-kDa translocator protein (TSPO) polymorphism explains differences in binding affinity of the PET radioligand PBR28. *J. Cereb. Blood Flow Metab. 32*, 1−5.
(35) Castellano, S., Taliani, S., Milite, C., Pugliesi, I., Da Pozzo, E., Rizzetto, E., Bendinelli, S., Costa, B., Cosconati, S., Greco, G., Novellino, E., Sbardella, G., Stefancich, G., Martini, C., and Da Settimo, F. (2012) Synthesis and biological evaluation of 4-phenylquinazoline-2-carboxamides designed as a novel class of potent ligands of the translocator protein. *J. Med. Chem. 55*, 4506−4510.
(36) Castellano, S., Taliani, S., Viviano, M., Milite, C., Da Pozzo, E., Costa, B., Barresi, E., Bruno, A., Cosconati, S., Marinelli, L., Greco, G., Novellino, E., Sbardella, G., Da Settimo, F., and Martini, C. (2014) Structure-activity relationship refinement and further assessment of 4-phenylquinazoline-2-carboxamide translocator protein ligands as antiproliferative agents in human glioblastoma tumors. *J. Med. Chem. 57*, 2413−2428.
(37) Pike, V. W. (1993) Positron-emitting radioligands for studies in vivo—probes for human psychopharmacology. *J. Psychopharmacol. 7*, 139−158.
(38) Laruelle, M., Slifstein, M., and Huang, Y. (2003) Relationships between radiotracer properties and image quality in molecular imaging of the brain with positron emission tomography. *Mol. Imaging Biol. 5*, 363−375.
(39) Waterhouse, R. N. (2003) Determination of lipophilicity and its use as a predictor of blood-brain barrier penetration of molecular imaging agents. *Mol. Imaging Biol. 5*, 376−389.
(40) Pike, V. W. (2009) PET Radiotracers: crossing the blood-brain barrier and surviving metabolism. *Trends Pharmacol. Sci. 30*, 431−440.
(41) Logan, J., Fowler, J. S., Volkow, N. D., Wolf, A. P., Dewey, S. L., Schlyer, D. J., MacGregor, R. R., Hitzemann, R., Bendriem, B., Gatley, S. J., and Christman, D. R. (1990) Graphical analysis of reversible radioligand binding from time-activity measurements applied to [*N*-^{11}C-methyl]-(−)-cocaine PET studies in human subjects. *J. Cerebr. Blood Flow Metab. 10*, 740−747.
(42) Innis, R. B., Cunningham, V. J., Delforge, J., Fujita, M., Gjedde, A., Gunn, R. N., Holden, J., Houle, S., Huang, S.-C., Ichise, M., Iida, H., Ito, H., Kimura, Y., Koeppe, R. A., Knudsen, G.-M., Knuuti, J., Lammertsma, A. A., Laruelle, M., Logan, J., Maguire, R. P., Mintun, M. A., Morris, E. D., Parsey, R., Price, J. C., Slifstein, M., Sossi, V., Suhara, T., Votaw, J. R., Wong, D. F., and Carson, R. E. (2007) Consensus nomenclature for *in vivo* imaging of reversibly binding radioligands. *J. Cereb. Blood Flow Metab. 27*, 1533−1539.
(43) Zoghbi, S. S., Anderson, K. B., Jenko, K. J., Luckenbaugh, D. A., Innis, R. B., and Pike, V. W. (2012) On quantitative relationships between drug-like compound lipophilicity and plasma free fraction in monkey and human. *J. Pharm. Sci. 101*, 1028−1039.
(44) Shultz, M. D. (2013) Setting expectations in molecular optimizations: strengths and limitations of commonly used composite parameters. *Bioorg. Med. Chem. Lett. 23*, 5980−5991.
(45) Cheng, Y., and Prusoff, W. H. (1973) Relationship between constant (K_i) and the concentration of inhibitor which causes 50% inhibition (IC_{50}) of an enzymatic reaction. *Biochem. Pharmacol. 22*, 3099−3108.
(46) Christman, D. R., Finn, R. D., Karlström, K., and Wolf, A. P. (1975) The production of ultra high specific activity ^{11}C-labeled hydrogen cyanide, carbon dioxide, carbon monoxide and methane via the ^{14}N(p,α)^{11}C reaction. *Int. J. Appl. Radiat. Isot. 26*, 435−442.
(47) Smith, D. (2008) Synthia gets extreme makeover courtesy of National Instruments, pp 24−25, ftp://ftp.ni.com/pub/branches/.../NIDaysBooklet.pdf.
(48) Bjurling, P., Reineck, R., Westerburg, G., Gee, A. D., Sutcliffe, J., and Långström, B. (1995) Synthia, a compact radiochemistry system for automated production of radiopharmaceuticals, in *Proceedings—Sixth Workshop on Targetry and Target Chemistry* (Link, J. M., Ruth, T. J., Eds.), pp 282−284, TRIUMF, Vancouver.
(49) Larsen, P., Ulin, J., Dahlström, K., and Jensen, M. (1997) Synthesis of [^{11}C]iodomethane by iodination of [^{11}C]methane. *Appl. Radiat. Isot. 48*, 153−157.
(50) Clark, J. D., Baldwin, R. L., Bayne, K. A., Brown, M. J., Gebhart, G. F., Gonder, J. C., Gwathmey, J. K., Keeling, M. E., Kohn, D. F., Robb, J. W., Smith, O. A., Steggerda, J.-A. D., and VandeBer, J. L. (1996) *Guide for the Care and Use of Laboratory Animals*, National Academy Press, Washington, DC.
(51) Gandelman, M. S., Baldwin, R. M., Zoghbi, S. S., Zea-Ponce, Y., and Innis, R. B. (1994) Evaluation of ultrafiltration for the free-fraction determination of single photon emission computed tomography (SPECT) radiotracers: β-CIT, IBF, and iomazenil. *J. Pharm. Sci. 83*, 1014−1019.